Research Square

Preprints are preliminary reports that have not undergone peer review.
They should not be considered conclusive, used to inform clinical practice,
or referenced by the media as validated information.

B. adolescentis Orchestrates CD143 + CAFs to Suppress Colorectal Tumorigenesis by Wnt signalling-regulated GAS1

Shujie Chen
Sir Run Run Shaw Hospital of Zhejiang University
Lina Fan
Second Affiliated Hospital of Zhejiang University School of Medicine
Yifeng Lin
Second Affiliated Hospital of Zhejiang University School of Medicine
Yadong Qi
Sir Run Run Shaw Hospital of Zhejiang University
Chaochao Xu
Second Affiliated Hospital of Zhejiang University School of Medicine
Qiwei Ge
Second Affiliated Hospital of Zhejiang University School of Medicine
Ying Zhang
Second Affiliated Hospital of Zhejiang University School of Medicine
Qiwen Wang
Sir Run Run Shaw Hospital of Zhejiang University
Dingjiacheng Jia
Second Affiliated Hospital of Zhejiang University School of Medicine
Jianmin Si
Sir Run Run Shaw Hospital of Zhejiang University
Liangjing Wang (wangljzju@zju.edu.cn)
Second Affiliated Hospital of Zhejiang University School of Medicine

Research Article

Keywords: Colorectal Cancer, Cancer-associated Fibroblasts, B. adolescents, scRNA-seq, CD143

Posted Date: May 6th, 2022

DOI: https://doi.org/10.21203/rs.3.rs-1607997/v1

License: This work is licensed under a Creative Commons Attribution 4.0 International License.
Read Full License

Abstract

Background

The interplay between gut microbiota and tumor microenvironment (TME) in the pathogenesis of colorectal cancer (CRC) is largely unknown. Here, we elucidated the functional role of *B. adolescentis* (*B.a*) and its possible mechanism on the manipulation of cancer-associated fibroblasts (CAFs) in CRC.

Methods

The relative abundance of *B.a* in the patients with CRC or the healthy individuals was analyzed. The role of *B.a* was evaluated in the CRC animal models. The single cell-RNA sequencing (scRNA-seq) was used to investigate the cell subsets in the TME. The expression level of Wnt signaling and its downstream GAS1 in CAFs were explored by western blot and *qRT-PCR*. Overexpression of GAS1 in NIH/3T3 was performed to investigate its effect on the subcutaneous tumor formation. Multi-immunofluorescence assay examined the expression level of CD143 and GAS1 on the tissue array.

Results

We found that *B. a* abundance was significantly reduced in CRC patients from two independent cohorts and the bacteria database of GMrepo. Supplementation with *B. a* suppressed $Apc^{Min/+}$ spontaneous or AOM/DSS-induced tumorigenesis in mice. scRNA-seq revealed that *B. a* facilitated a new subset $CD143^{+}$CAFs to highly express GAS1 and $GAS1^{+}$CAFs existed a suppressive effect. Mechanistically, GAS1 were activated by the Wnt/β-catenin signaling in $CD143^{+}$CAFs. *B. a* abundance was correlated with the expression level of CD143 and GAS1. The level of $CD143^{+}$CAFs predicted the more satisfied survival in CRC patients.

Conclusions

These results highlight that *B. a* induced a new subset $CD143^{+}$CAFs and provides a novel therapeutic target for probiotic-based modulation of TME in CRC.

Introduction

Colorectal cancer (CRC) is the third most common cancer and has ranked the third leading cause in cancer-associated death globall[1]. The initiation and progression of CRC was related with multiple factors including genetic or epigenetic changes, environmental factors, and intestinal microbiota[2,3]. Microbiota disorder leads to intestinal homeostasis imbalance, and thereby induces epithelial dysplasia and carcinogenesis. Some “CRC-promoting” bacteria have been studied in CRC such as *Fusobacterium*

nucleatum[4–6], *Peptostreptococcus anaerobius*[7] and *Bacteroides fragile*[8,9]. Previous studies demonstrated that "Cancer-suppressing" bacteria could inhibit cell proliferation[10], inducing cancer cell apoptosis[11] and produce anti-cancer compounds[12]. However, the direct evidence supporting the use of probiotics for preventing CRC is lacking.

Bifidobacterium adolescentis (*B. adolescentis, B.a*) is a gram-positive anaerobic bacterium belonging to *Actinobacteria* phylum. Studies showed that *B. a* protected mice from *Yersinia* and toxigenic *E. coli* infection, and antagonized harmful bacteria growth[13,14]. Tze *et,al* found that *B. a* could induce Th17 cells without inflammation in the murine intestine[15]. Our previous study showed that *B. a* ameliorated chronic colitis by regulating iTreg/Th2 response[16]. Low *Bifidobacterium* abundance in the lower gut microbiota was associated with *Helicobacter Pylori*-related gastric cancer[17]. Transplantation with *Bifidobacteria* could improve the effect of melanoma immunotherapy[18].

Microbiota-host tumor microenvironment (TME) interaction plays a crucial role in the pathogenesis of CRC. Some "harmful bacteria" recruited myeloid-derived suppressor cells (MDSCs) or Treg cells in the tumor[19,20]. Some "beneficial bacteria" can enhance the anti-tumor immune response. *Bifidobacterium* increased the antigen presentation ability of dendritic cells[21]. Cancer-associated fibroblasts (CAFs) are the main cellular components of the TME[22]. Studies suggested that CAFs can modulate tumor stroma microenvironment and their functional heterogeneity are the potential therapeutic targets for cancer. However, the role of *B. a* in the CRC microenvironment has not been well explored.

Here, we found that the abundance of *B. a* was significantly reduced in patients with CRC. Supplementation with *B. a* suppressed colonic tumorigenesis in AOM/DSS model and $Apc^{Min/+}$ mice. Single-cell RNA sequencing (scRNA-seq) revealed that *B. a* facilitated a subset $CD143^{+}$CAFs which highly expressed GAS1 to suppress CRC. Mechanistically, GAS1 was activated by Wnt/β-catenin signaling in $CD143^{+}$CAFs. These results highlighted *B. a* induced a new subset $CD143^{+}$CAFs and provided a novel therapeutic target for probiotic-based modulation of TME in CRC.

Materials And Methods

Human sample collection

Fresh stool samples were obtained from 71 patients with CRC and 40 healthy subjects at the Sir Run Run Shaw Hospital of Zhejiang University School of Medicine (cohort 1). Fresh tumor and paired normal tissues were obtained from 99 patients with CRC who underwent surgical resection at Sir Run Run Shaw Hospital (cohort 2). All samples were refrigerated at liquid nitrogen until use. Fresh CRC tissues and their paired normal tissue were obtained from 20 patients with CRC who underwent surgical resection at Sir Run Run Shaw Hospital (cohort 3). The tissue array tissues came from the patients with CRC at the Second Affiliated Hospital of Zhejiang University School of Medicine (cohort 4). Clinical Research Ethics Committee of the Sir Run Shaw Hospital, Zhejiang University School of Medicine approved the protocol

(20211103-35). All aspects of the study were conducted in accordance with the principles of the Declaration of Helsinki.

GMrepo database analysis

The GMrepo revealed the relative abundance of human gut microbiota in the people with different diseases. The abundance data of *B. a* in the patients with CRC and the healthy people were downloaded from GMrepo database using GMrepo RESTful APIs for R (version 3.6.1 https://www.r-project.org) and the RStudio (version 1.1.442 https://www.rstudio.com) software. We assessed data quality by consulting the description of the samples and supplementary data of related publications. Then, the relative abundance of *B. a* for the healthy and CRC patients was analyzed.

Bacteria strain and culture

B. adolescentis ATCC15703 was purchased from American type culture collection (ATCC, USA). V4 of 16S ribosomal RNA sequencing was performed to confirm bacterial strain at the species level. The bacteria were cultured in anaerobic modified Reinforced Clostridium Medium (BD Difco, Sparks, MD, USA) under an atmosphere of 10% H2, 10% CO2, and 80% N2 (AW500SG anaerobic workstations, ELECTROTEK, England) for 48 h. The non-pathogenic commensal intestinal bacteria, *E. coli* strain *DH5a* (Code No.9057, Takara), which was used as a negative control, was cultured in Luria-Bertani medium (Cat. #A507002 Sangon Biotech) at 37℃. When the optical density (OD) at 600 nm of *B. a* reached 1.0, the cultures were centrifuged at 3000 rpm for 5 min at 4℃ and then washed twice with sterile anaerobic PBS, then resuspended at a final concentration of 1×10^9 CFU/300μl under strictly anaerobic conditions.

Animal use and care

All animal studies were approved by the Institutional Animal Care and Use Committee (IACUC) of Zhejiang University (ZJU) (IACUC-02102214). All animal experiments strictly adhered to protocols, policies, and ethical guidelines formulated by our IACUC. $Apc^{Min/+}$ mice were purchased from Nanjing Biomedical Research Institute of Nanjing University (NBRI), China. BALB/C nude mice and C57L/B6 mice were purchased from Shanghai SLAC Laboratory Animal, China. All mice were maintained in ventilated cages with 12-hour light/dark cycles, constant temperature and humidity, enriched water and ad libitum feeding under specific pathogen-free (SPF) conditions.

Carcinogen-induced cancer model

6-week-old male C57BL/6 wildtype mice were purchased from Shanghai SLAC Laboratory Animal, China. Before bacterial intragastric administration, mice were fed with 2 mg/ml streptomycin (Cat. #MB1275, Meilunbio) in the drinking water for 7 days to ensure the consistency of regular microbiota and facilitate *B. a* colonization as previous study reported[23]. Mice were given a cycle of one single intraperitoneal injection of azoxymethane (AOM, Cat. #A5486, sigma, 10 mg/kg body weight) at first week, then followed by three cycles of 5 days of 2.5% DSS (Cat. #160110, MP Biomedicals) administration. At the intervals,

mice were performed administration of 1×10^9 colony forming units (CFU) of *B. a*, *E. coli* or the same volume of PBS three times per week for 120 days for the development of neoplastic lesions.

Spontaneous adenomatous mice

Prior to intragastric bacteria administration, Male C57BL/6J $Apc^{Min/+}$ mice (6-8 week of age, 20g) were fed with 2 mg/mL streptomycin in the drinking water for 7 days to ensure the consistency of regular microbiota and facilitate *B. a* colonization. $Apc^{Min/+}$ mice were randomly assigned to three groups. Mice in *B.a* and *E. coli* groups were administrated 1×10^9 CFU *B. a* or *DH5a* suspended in 300μl sterile anaerobic PBS, respectively, every 2 days for 3 months. The control group was administrated with PBS. Two cycles of 10-day 1% DSS was given to accelerate tumorigenesis. The body weight of mice was measured every week and mice anus prolapse were observed at the final month.

At the indicated time intervals, colon and spleen tissues were harvested after fasting. Colon tissues were photographed and the number and size of tumors were measured. Tumor sizes (diameter) were quantified as <1 mm, 1-2 mm, 2-3 mm, or >3 mm. Tumor load was calculated as the sum of all tumor diameters in a single mouse. Spleen tissues were photographed and weight measured.

Genomics library and single cell RNA sequencing

The prepared single-cell suspensions were loaded to 10× Chromium to capture enough single cell according to the 10×Genomics Chromium Single-Cell 3' kit (V3) manufacturer's instructions. The reverse transcription, cDNA amplification and library construction steps were performed according to the standard protocol (10× Genomics). Sequencing libraries were sequenced on an Illumina NovaSeq 6000 sequencing system (paired-end multiplexing run,150bp) by LC-Bio Technology co.ltd (HangZhou, China) at a minimum depth of 20,000 reads per cell.

We excluded contaminating lineage cells and low-quality cells, and finally obtained 14,736 cells. Unsupervised graph clustering divided infiltrating cells into 24 groups based on gene expression pattern. Cells were divided into 6 groups according to their top expression markers, as previous studies reported[24-26]. T cells were marked by Cd3e, Cd3d, Cd3g, Trbc1, Trbc2, Icos. Myeloid cells were marked by Cd14, Csf1r, Fogr3, Adgre1. Fibroblast cells were Col1a2, Col1a1, Dcn, Sparc. Cancer cells were Epcam, Cdh1, Krt8, Krt18. Endothelial cells were marked by Pecam1, Cdh5, Ramp2, Eng. B cells were marked by Cd79a, Cd79b, Cd19, Ms4a1. According to the Fibroblast cell group, unsupervised graph clustering divided infiltrating cells into 12 groups based on gene expression. Cell types finally identified were plotted in t-SNE.

DNA extraction and bacteria DNA quantification

Bacterial DNA from human fecal contents were extracted using QIAGEN stool kits (Cat. #51604, QIAGEN, Germany), and bacterial genomic DNA from human tissues were extracted using QIAGEN DNA mini kits (Cat. #56304) according to the manufacturers' protocol. Quantitative real-time PCR was performed to

assess the *B. a* genes, Universal Eubacteria 16S and PGT using a ROCHE LightCycler®480 System (Rotor gene 6000 Software, Sydney, Australia). Each reaction was performed in triplicate with SYBR Premix Ex Taq (Cat. #RR820A, Takara, Japan), primers and 100ng template gDNA. Relative abundance was calculated by -ΔCt method. Universal Eubacteria 16s was used as internal reference gene for stool samples. The PGT gene was used as internal control for tissue samples. Primers used are listed in the **Supplementary Table S1**.

Subcutaneous tumor models

Female BALB/C nude mice (3-4 week of age, 15 g) were kept in SPF conditions. CAFs from CRC patient were incubated with *B. a* (MOI=10:1) for 48 hours, then HCT-116 cells and CAFs were washed twice with PBS and harvested using trypsin-EDTA solution (Cat. # GNM25200, Genom). 3×10^6 HCT-116 cells were mixed with *B.a* treated-CAFs (MOI=10:1) or PBS treated-CAFs with 25 μL matrigel matrix (Cat. #354234, Corning Biocoat), and then injected (100 μL per mouse) subcutaneously into the right flank of nude mice. After 7 days implantation, tumor volume was monitored every two days and calculated as follows: $Volume=0.54\times L\times W^2$, where L is the longest diameter and W is the shortest diameter. At the terminal time, the tumor weights were recorded.

Histopathological analysis

Colorectal tumors or subcutaneous tumors were fixed overnight with 10% formalin at room temperature and then embedded in paraffin. Sections of 5 μm were stained with hematoxylin and eosin (H&E) for pathological analysis. For immunohistochemistry, sections of paraffin-embedded tissue were stained by PCNA-specific antibody (Cat. #GB11010-1, diluted 1:1000, Servicebio, China), α-SMA-specific antibody (Cat. #GB13044, diluted 1:1000, Servicebio), CD31-specific antibody (Cat. #GB11063-2, diluted 1:1000, Servicebio) and Ki67-specific antibody (Cat. #GB111141, diluted 1:1000, Servicebio), and visualized by DAB (Cat. #G1212, Servicebio) staining according to manufacturer's instructions.

Tumor sample dissociation and single cell suspension preparation

Mice colon tumor tissues were acquired from AOM/DSS model with or without *B. a*. Tumors were cut into 0.5 mm^2 fragments. Tumor samples were digested for 40 min at 37 °C in Hanks buffer (Cat. #MA0041, Meilunbio) containing 5% FBS (Cat. #10270, Gibco), Collagenase IV (200U/ml, Cat. #A005318, Sangon Biotech) and DNase I (120 U/ml, Cat. #B300065, Sangon Biotech), as previous study reported. Samples were typically fully dissociated at this step and filtered through a 40 mM cell strainer. Cells were centrifuged down at 500 g for 10 min and resuspended in 1 mL of ACK lysis (Cat. #R1010, Solarbio) and placed on ice for 3 min. Cells were spun down at 700 g for 5 min and placed on ice. The dead cells were removed by Dead Cell Removal MicroBeads (Cat. #MACS 130-090-101, Germany) and Miltenyi ® Dead Cell Removal Kit (Cat. #MACS 130-090-101, Germany). In the end, the cells were resuspended in PBS containing 0.04% BSA and centrifuged at 300 g for 3 min at 4 °C. The cell viability needed to be above 85% determined by trypan blue staining (Cat. #MA0130, Meilunbio) using an automated counter, finally subsequently adjusted the cell concentration to 700-1200 cells/μL.

Cell culture

HCT-116 human colon cancer cells were obtained from the ATCC at the beginning of this project. Cells were maintained at 37 ℃ under 5% CO2 in McCoy's 5A (Cat. #GNM16600, Genom) with 10% (vol/vol) FBS (Cat. #10270, Gibco) supplemented with 1% (vol/ vol) penicillin and streptomycin (Cat. #P1400, Solarbio) and maintained in culture for a maximum of 2 months or 10 passages. Murine embryonic fibroblast NIH/3T3 were also obtained from the ATCC at the beginning of our study and maintained in culture for a maximum of 2 months or 10 passages. All cells tested negative for Mycoplasma contamination and were authenticated on the basis of short tandem repeats fingerprinting before use.

Fibroblast (CAFs and normal tissue–associated fibroblast) isolation

The fresh tumor or normal colon tissues were cut into small blocks with a diameter of 2 mm and subsequently seeded on the surface of culture flask containing DMEM supplemented with 20% FBS (Gibco) and 1% penicillin/streptomycin (Solarbio). Culture flask was inverted and maintained at 37 ℃ under 5% CO2 for 1 hour until the culture flask was turned over. The adherent cells were continuously cultured in DMEM with 20% FBS for approximately 2 weeks (tumor tissues) or 3 to 4 weeks (paired normal colon tissues). The culture medium was replaced every three days. Large groups of fibroblasts (morphologically spindle-shaped cells became apparent after 2 weeks and they were validated by western blot and immunofluorescence staining.

Cell culture in the presence of *B. adolescentis*

CAF cells were digested by trypsin-EDTA solution (Cat. #GNM25200, Genom) slightly, then they were seeded at a density of 2×10^5 cells per well in 6-well plate and cultured in DMEM with 10% (vol/vol) FBS (Gibco) overnight. Then they were incubated with *B. a* at a MOI of 100:1 for 48 h. Finally, CAF cells were digested by trypsin-EDTA solution (Cat. #GNM25200, Genom) for further analysis.

HCT-116 cells were subsequently seeded at a density of 2×10^3 cells per well with the *B.a* or PBS incubated-CAFs(MOI=1:10) in the 96-well plate for 24, 48,72 hours, then the Cell viability was analyzed using a Cell Counting Kit (CCK-8, Cat. #CK04, Dojindo) according to the manufacturer's instructions at different time points. Briefly, after removing the medium, cells were incubated with CCK8 for 2 hours and the absorbance was determined at 450 nm, each test was repeated five times.

For LiCl stimulation assay, CAFs were incubated with Wnt signaling agonist lithium chloride (LiCl) (20 mmol/L) for 24 h, then the expression of c-Myc, Cyclin D1 and GAS1 were analyzed.

Statistical analysis

Data were expressed as mean ± Standard Deviation (SD) and were analyzed by paired or unpaired Student's t test, one-way ANOVA test, Mann Whitney test or spearman correlation analysis. A P value < 0.05 was considered statistically significant. Statistical analyses were performed using GraphPad Prism

5.04 software (GraphPad Software, Inc., La Jolla, CA, USA) and SPSS 19.0 for Windows (SPSS Inc., Chicago, IL, USA).

Results

B. adolescentis was decreased in CRC patients and suppressed tumorigenesis in mice

We examined the fecal *B. a* abundance in healthy populations and patients with CRC (cohort 1). Quantitative PCR showed fecal *B. a* abundance was significantly lower in CRC patients than that in the healthy controls (Fig. 1a). In addition, we found that *B. a* abundance was decreased in tumor tissues compared to their adjacent normal mucosa (cohort 2) (Fig. 1b). Consistently, the GMrepo database indicated that fecal *B. a* abundance in CRC patients was significantly lower as compared to healthy individuals (Fig. 1c). These results suggested that the abundance of *B. a* was decreased in CRC patients.

We then evaluated the effect of *B. a* in CRC. AOM/DSS-induced carcinogenesis model mimics colonic tumor progression caused by chronic colitis as seen in inflammatory bowel disease (IBD). Six-week-old C57BL/6 mice were injected with AOM (10 mg/kg) at the first week, followed by three cycles of 2.5%DSS and oral administration with *B.a or E. coli* for 120 consecutive days. *B. a* supplement mice had an obvious reduction in tumor number and load as compared with those gavage with *E. coli* or PBS (Fig. 1d,e). The lower expression of proliferative marker PCNA and tumor angiogenesis marker CD31 was observed in *B. a* group (Fig. 1f-h). Immunohistochemistry staining of the fibroblast marker of α-SMA was highly expressed in the tumor from *B. a*-gavage mice (Fig. 1i). The spleen weight showed an obvious decrease in *B. a* group (Fig. 1j).

Six-week-old $Apc^{Min/+}$mice were orally gavage with *B. a* or *E. coli* for 90 consecutive days including two cycles of 1%DSS administration. We observed consistent tumor-suppressive effect of *B. a* in $Apc^{Min/+}$ spontaneous tumor mice (Fig. 1k-n and **Fig. S1a**). Collectively, our results indicated that *B. a* could suppress $Apc^{Min/+}$ spontaneous and AOM/DSS-induced tumorigenesis in mice.

B. adolescentis recruited fibroblasts to suppress colonic tumorigenesis

To explore the tumor infiltrating cells during CRC progression, we analyzed cell populations identified from AOM/DSS-induced colon tumors by single cell RNA-sequencing (scRNA-seq) (Fig. 2a). We obtained 14,736 cells and unsupervised graph clustering divided infiltrating cells into 24 groups based on gene expression pattern (Fig. 2b,c). Furthermore, we labeled cell subsets with canonical markers and divided them into six groups including B cells, endothelial cells, cancer cells, fibroblast cells, myeloid cells and T cells, which were plotted in t-SNE (Fig. 2d-f and **Fig. S2**). A total of 4898 cells were classified into myeloid populations, accounting for 33.23% of the total cells. Based on scRNA-seq data, *B. a* treatment changed the proportion of these six defined cell types. *B. a* supplement obviously increased fibroblast cells (72.14%) while decreased the B cells (30.22%) (Fig. 2g). Biological function and cell-cell interaction network in the main six cell types were shown in online supplementary Fig. 3 by iTALK R packages, which

demonstrated the microbiota might regulate the TME in CRC by regulating cell-cell interaction. These results indicated that fibroblast cells were involved in the effect of *B. a* in CRC.

To confirm whether fibroblasts mediate the tumor suppressive effect of *B. a in vitro*, we separated and identified cancer associated fibroblasts (CAFs) from CRC patients by western blot or immunofluorescence (**Fig. S4**). CAFs were then incubated with *B. a* or *E. coli* for 48 h, and co-cultured with HCT-116 cells. We found that *B. a*-treated CAFs significantly inhibited CRC cell proliferation compared with the *E. coli* or PBS control groups (Fig. 2h). To confirm whether *B. a*-treated CAFs suppressed the tumor growth *in vivo*, we mixed the HCT-116 CRC cells and CAFs with or without *B. a* treatment and co-injected into the nude mice. We observed that *B. a*-treated CAFs had an obvious growth inhibitory effect on HCT-116 tumors in nude mice. The reduction of cell proliferative and angiogenesis ability was verified by the staining with Ki67 and CD31 (Fig. 2i-k). Collectively, these data demonstrated that *B. a*-treated CAFs suppressed tumorigenesis *in vivo* and *in vitro*.

CD143 $^+$ CAFs was activated by B. adolescentis in vivo **and** in vitro

As *B. a* treatment induced more functional CAFs in CRC progression, we proposed that these distinctive CAFs might present with specific molecular signatures. We further analyzed the CAFs subsets by scRNA-seq, and found that unsupervised graph clustering divided CAFs into 12 groups (Fig. 3a,b). Furthermore, we used conventional fibroblast markers and other surface markers to distinguish them and acquired five CAF subsets including C1(PDGFRβ), C2(collagen I), C3(MYH11), C4(CD143), C5(CD36) (Fig. 3c and **Fig. S5**). Combining with the t-SNE result, we found that the subset C4 (CD143) was mainly located in the *B.a*-treated group while other subsets failed to distinguish them (Fig. 3d,e). These results suggested that *B. a* could induce the functional CD143$^+$ CAFs *in vivo*.

To confirm the existence of CD143$^+$ CAFs, the dual positive of SMA and CD143 cells were stained by immunofluorescence assay in the tumor tissues from patients with CRC (Fig. 3f). We further explored the percentage of total CAFs (Epcam$^-$CD31$^-$AFP$^+$) and CD143$^+$ CAFs (Epcam$^-$CD31$^-$AFP$^+$CD143$^+$) by flow cytometry. CRC tissues had more CAFs while less CD143$^+$ CAFs than their paired normal tissues (**Fig. S6a,b**). In addition, the *B. a*-treated CAFs induced more CD143$^+$ CAF cells in the tumor tissues from nude mice (**Fig. S6c**). To explore whether *B. a* could induce the CD143$^+$ CAFs *in vitro*, we co-cultured the CAFs with *B. a* or *E. coli* for 48 h. We observed that *B. a* increased the expression level of CD143 in CAFs compared with *E. coli* or PBS control group by immunofluorescence, western blot and *RT-qPCR* assays (Fig. 3g-h). Taken together, these results revealed that *B. a* could recruit the subset CD143$^+$ CAFs *in vivo* and *in vitro.*

CD143 $^+$ CAFs was highly expressed with GAS1 in response to B. adolescentis **treatment**

To explore how CD143$^+$CAFs inhibiting CRC progression, we performed different gene expression (DGE) between the PBS and *B.a* groups in AOM/DSS-treated mice. We found that growth arrest specific 1 (GAS1) was the significantly increased gene in the *B.a* supplement group, and GAS1 mainly expressed in

the CD143^{+}CAFs subset (Fig. 4a,b). The expression of GAS1 in CD143^{+}CAFs had 8-fold increase compared to the CD143^{-}CAFs (Fig. 4c). Furthermore, we observed more SMA^{+}GAS1^{+} dual positive cells in the *B.a*-treated group (Fig. 4d).

To confirm that *B. a* increased the expression of GAS1 in CAFs *in vitro*, we co-cultured CAFs with *B. a* or *E. coli* for 48 h. Results demonstrated that *B. a* upregulated the expression of GAS1 by western blot and *RT-qPCR* (Fig. 4e,f). These data suggest that *B. a* treatment induced CD143^{+} CAFs to highly express with GAS1. To investigate the suppressive function of GAS1 in CAFs on CRC, we acquired the GAS1-overexpressed NIH/3T3 cells (**Fig. S6d**). We found that overexpression of GAS1 in NIH/3T3 cells efficiently inhibited the growth of MC38 cells in nude mice. The cell proliferative and angiogenesis ability was reduced after GAS1-overexpression (Fig. 4g-i), which suggest that GAS1^{+}CAFs existed a suppressive effect in CRC.

Wnt/β-catenin signaling was involved in the CD143 $^{+}$ CAFs induction by B. adolescentis

To explore the regulatory mechanism of GAS1 expression, we analyzed the online translatory predictor datasets of UCSC and JASPAR. 14 translator factors were collected according to these two datasets merged files (Fig. 5a). We narrowly analyzed the translator factors of the five CAFs subsets and found the expression of TCF4 and NFKB1 were significantly increased in the group C4 (CD143) (Fig. 5b). TCF4 was the most convinced translator factor to activate GAS1. The predictor of C4 subset by KEGG pathway also confirmed that Wnt pathway was activated in the CD143^{+}CAFs (Fig. 5c). Furthermore, we found that the protein level of NF-κB pathway molecule p-p65 was not changed in *B. a*-treated CAFs and the AOM/DSS-induced tumor tissues (**Fig. S7a,b**). The TGF-β pathway had no significant difference in the tumor tissues between PBS group and *B. a* group or between PBS and *B. a*-treated CAFs (Fig. 5d and **Fig. S7c**).

To further conduct whether the Wnt/β-catenin pathway was activated by *B. a*, we co-cultured the CAFs with *B. a* or *E. coli* and found the Wnt/β-catenin downstream genes of *Tcf4*, *Axin2*, *Cyclin D1* and *c-Myc* increased in the *B. a*-treated CAFs (Fig. 5e). The increased expression level of c-Myc and Cyclin D1 was confirmed by western blot analysis in the *B.a* group (Fig. 5f). In contrast, *B. a* had no effect on the HCT-116 CRC cells (**Fig. S7d**).

The induction of nuclear β-catenin translocation indicated that Wnt/β-catenin pathway was activated by *B. a* in the CAFs (Fig. 5g). We proposed that GAS1 and CD143 are the downstream of the Wnt/β-catenin signalling. We found that lithium chloride (LiCl) (20 mmol/L), the Wnt signaling agonist, increased the expression level of GAS1, CD143 and Wnt downstream targets c-Myc and Cyclin D1 (Fig. 5h). To investigate whether Wnt/β-catenin signaling pathway was activated by TCF4 in *B. a*-treated CAFs, we performed the TCF4 deficient assay (**Fig. S7e**). We observed that knockdown of TCF4 obviously inhibited the expression of GAS1 and CD143 by western blot assay and attenuated the activation of Wnt/β-catenin pathway by *B. a* in CAFs (Fig. 5i,j). These data indicated that Wnt/β-catenin signaling was involved in CD143^{+} CAFs induction by *B. a in vitro.*

CD143 $^{+}$ CAFs predicated better survival in CRC patients and B. adolescentis **abundance was correlated with the expression of CD143 and GAS1**

We further evaluated clinical association between *B. a*, CD143 and GAS1 in our clinical cohorts and TCGA dataset. We defined two groups with low or high abundance of *B. a* by the DNA level (-ΔCT =-15) and found the abundance of *B. a* was related to the mRNA expression level of CD143 in cohort 3 (Fig. 6a). The high *B.a* abundance group enriched more percentage of $CD143^{+}$CAFs by flow cytometry assay (Fig. 6b,c). CD143 level was decreased in the late-stage tumors in cohort 2 (Fig. 6d). The relative expression of GAS1 was reduced in cancer tissues compared with the normal tissue (The cohort 2 and the TCGA dataset) (Fig. 6e,f). The high *B. a* abundance group had a relative high level of GAS1 mRNA (cohort 2 and cohort 3) (Fig. 6g,h). The abundance of *B. a* was associated with higher $SMA^{+}CD143^{+}$ or $SMA^{+}GAS1^{+}$ dual positive cells in cancer tissues, as determined by immunofluorescence staining (cohort 2) (Fig. 6i).

We examined the number of $CD143^{+}$α-SMA^{+} dual positive cells in 80 patients with CRC (cohort 4). Results showed that the overall survival percentage was increased in the high number of α-$SMA^{+}CD143^{+}$ cells group (Fig. 6j-l), which suggested the subset $CD143^{+}$CAFs could be a promising marker to predicate a better survival outcome.

Discussion

Studies demonstrated that some specific bacteria regulated the tumor microenvironment in the progression of CRC and exerted a promising therapeutic function. Herein, we identified that *B. a* suppressed colonic tumorigenesis and induced $CD143^{+}$ CAFs with highly expressed GAS1 through Wnt/β-catenin pathway. scRNA-seq revealed that *B. a* treatment recruited more CAFs in the tumor tissues (Fig. 2). Studies suggested that different fibroblast subsets exerted opposite functions in cancer progression[27]. CAFs can promote tumor progression through a variety of mechanisms, such as secreting cytokines and exosomes to mediate intercellular communication, inducing tumor cell epithelial-mesenchymal transition, promoting blood vessel formation and immune escape[22]. However, certain CAFs subgroups inhibit tumorigenesis. Non-selective CAFs deletion in pancreatic tumor could promote cancer angiogenesis[28]. $Meflin^{+}$ CAFs surrounded the pancreatic tumor inhibited the cancer progression[29]. The decreased $CD68^{+}$ CAFs were related with the infiltration of regulatory T cells in oral carcinoma with poor prognosis[30].

Recent studies suggest that CAFs are heterogeneous and contain different subpopulations with distinct phenotypes and functions[31,32]. The heterogeneity of CAF subsets is tumor-type dependent. Oral squamous cell carcinoma can be divided into CAF-N and CAF-D[33]. The CAFs of breast cancer were divided into mCAF, dCAF, vCAF and cCAF by single-cell sequencing[34]. Our study discovered 5 subsets of CAFs, including C1(PDGFRβ), C2(collagen I), C3(MYH11), C4(CD143), C5(CD36). The new subset CAFs expressing CD143 was specifically activated by *B. a in vivo* and *in vitro* (Fig. 3). CD143 is the

angiotensinase, which is expressed in endothelial cells[35] and dendritic cells[36]. The definition of CAFs is generally based on the markers of α-SMA, fibroblast activation protein (FAP), platelet-derived growth factor (PDGFRβ) and so on[22]. However, the above-mentioned markers are not specific for CAFs. For example, FAP can be expressed in bone marrow, skeletal muscle, pancreas and other tissues. Inadvertently removing FAP^+ cells can lead to anemia and muscle atrophy[37].

GAS1, called growth arrest-specific 1, is located on the membrane of cells and belongs to the glial cell-derived neurotrophic factor ligand (GDNF) family α receptor (GFRα), expressed in a variety of epithelial cells and fibroblasts[38]. GAS1 was determined as a negative regulator of oncogenesis and metastasis in CRC. Mechanistically, GAS1 negatively regulated the aerobic glycolysis, a process that contributed to tumor progression and metastasis[39]. However, the role of GAS1 on CAFs are still unclear. Our study demonstrated that the $CD143^+$ CAF subset highly expressed GAS1 compared with the $CD143^-$ CAF subset (Fig. 4). GAS1 was as a cell marker and the effect molecule to negatively suppress the CRC tumor proliferation. Therefore, the GAS1 highly expressed $CD143^+$ CAF subset might be a new predictive marker or a therapeutic target for CRC.

Recent studies have revealed a variety of upstream signals that regulate the CAFs differentiation. Blocking the TGF-β signal in the breast cancer microenvironment could promote the formation of immunoregulatory fibroblast subpopulations[40]. The granular protein from liver macrophages activated liver fibroblasts[41]. A previous study showed that GAS1 is induced by WNTs[42]. In our study, the datasets and the scRNA-seq together revealed that TCF4 was the most convinced translatory factor to activate GAS1. Wnt/β-catenin signaling involves in the induction of $CD143^+$ CAFs by *B. a in vitro* (Fig. 5). Wnt signal in different cells plays a completely different role. Mutation-induced activation of WNT/β-catenin signaling is a frequent driver event in human cancer[43]. Wnt signal activation in CAFs of colon cancer can promote the contact of CAFs with cancer cells and inhibit epithelial-mesenchymal transition[44].

Conclusions

Our study found supplementation with *B. adolescentis* suppressed $Apc^{Min/+}$ spontaneous or AOM/DSS-induced tumorigenesis in mice. Single-cell RNA sequencing (scRNA-seq) revealed that *B. adolescentis* facilitated a new subset $CD143^+$CAFs with highly expressed GAS1 in the tumor microenvironment to suppress CRC. Wnt/β-catenin signaling was activated in $CD143^+$CAFs induced by *B. adolescentis*. These results highlight that *B. adolescentis* induced a new subset $CD143^+$CAFs and it could be a promising marker to predicate a better survival outcome, which provides a novel therapeutic target for probiotic-based modulation of tumor microenvironment in CRC.

Declarations

Acknowledgments

We are grateful to Dr. Wei Liu (Zhejiang Academy of Agricultural Sciences, China) for providing the culture method of *B. adolescentis*.

Author contributions

S. Chen analyzed data, drafted and revised the manuscript. L. Fan performed the experiments, analyzed data and drafted the manuscript. Y. Lin performed experiments and analyzed data. Y. Qi performed the database analysis. C. Xu and Q. Ge collected human samples. Y. Zhang, Q. Wang, D. Jia collected the data. J. Si revised and commented the manuscript. L. Wang designed, supervised the study and revised the manuscript.

Funding

This work was supported by the National Natural Science Foundation of China (grant no. 82072623, to L. Wang), Zhejiang Province Natural Science Foundation (grant no. LZ22H160002, to L. Wang) and Zhejiang Province Public Welfare Technology Research Project (grant no. LGD21H160002, to S. Chen).

Availability of data and materials

The datasets used and analyzed during the current study are available within the manuscript and its additional files.

Ethical approval and consent to participate

This research was approved by the Clinical Research Ethics Committee of the Sir Run Shaw Hospital, Zhejiang University School of Medicine. The in vivo assay using mice were approved by the Institutional Animal Care and Use Committee (IACUC) of Zhejiang University.

Consent for publication

Not applicable.

Competing interests

The authors declare that they have no conflicts of interest.

References

1. 1. Siegel RL, Miller KD, Fuchs HE, Jemal A. Cancer Statistics, 2021. CA: a cancer journal for clinicians 2021;71(1):7–33.
2. 2. Carr PR, Weigl K, Jansen L, Walter V, Erben V, Chang-Claude J, et al. Healthy Lifestyle Factors Associated With Lower Risk of Colorectal Cancer Irrespective of Genetic Risk. Gastroenterology 2018;155(6):1805-15 e5.

3. 3. Louis P, Hold GL, Flint HJ. The gut microbiota, bacterial metabolites and colorectal cancer. Nat Rev Microbiol 2014;12(10):661 – 72.
4. 4. Rubinstein MR, Baik JE, Lagana SM, Han RP, Raab WJ, Sahoo D, et al. Fusobacterium nucleatum promotes colorectal cancer by inducing Wnt/beta-catenin modulator Annexin A1. EMBO Rep 2019;20(4).
5. 5. Yu T, Guo F, Yu Y, Sun T, Ma D, Han J, et al. Fusobacterium nucleatum Promotes Chemoresistance to Colorectal Cancer by Modulating Autophagy. Cell 2017;170(3):548 – 63 e16.
6. 6. Chen S, Su T, Zhang Y, Lee A, He J, Ge Q, et al. Fusobacterium nucleatum promotes colorectal cancer metastasis by modulating KRT7-AS/KRT7. Gut Microbes 2020;11(3):511 – 25.
7. 7. Tsoi H, Chu ESH, Zhang X, Sheng J, Nakatsu G, Ng SC, et al. Peptostreptococcus anaerobius Induces Intracellular Cholesterol Biosynthesis in Colon Cells to Induce Proliferation and Causes Dysplasia in Mice. Gastroenterology 2017;152(6):1419-33 e5.
8. 8. Dejea CM, Fathi P, Craig JM, Boleij A, Taddese R, Geis AL, et al. Patients with familial adenomatous polyposis harbor colonic biofilms containing tumorigenic bacteria. Science 2018;359(6375):592-7.
9. 9. Gu T, Li Q, Egilmez NK. IFNbeta-producing CX3CR1(+) macrophages promote T-regulatory cell expansion and tumor growth in the APC(min/+) / Bacteroides fragilis colon cancer model. Oncoimmunology 2019;8(12):e1665975.
10. 10. Nowak A, Paliwoda A, Blasiak J. Anti-proliferative, pro-apoptotic and anti-oxidative activity of Lactobacillus and Bifidobacterium strains: A review of mechanisms and therapeutic perspectives. Crit Rev Food Sci Nutr 2019;59(21):3456-67.
11. 11. Konishi H, Fujiya M, Tanaka H, Ueno N, Moriichi K, Sasajima J, et al. Probiotic-derived ferrichrome inhibits colon cancer progression via JNK-mediated apoptosis. Nature communications 2016;7:12365.
12. 12. Li Q, Hu W, Liu WX, Zhao LY, Huang D, Liu XD, et al. Streptococcus thermophilus Inhibits Colorectal Tumorigenesis Through Secreting beta-Galactosidase. Gastroenterology 2021;160(4):1179-93 e14.
13. 13. Frick JS, Fink K, Kahl F, Niemiec MJ, Quitadamo M, Schenk K, et al. Identification of commensal bacterial strains that modulate Yersinia enterocolitica and dextran sodium sulfate-induced inflammatory responses: implications for the development of probiotics. Infect Immun 2007;75(7):3490-7.
14. 14. Resta-Lenert S, Barrett KE. Live probiotics protect intestinal epithelial cells from the effects of infection with enteroinvasive Escherichia coli (EIEC). Gut 2003;52(7):988 – 97.
15. 15. Tan TG, Sefik E, Geva-Zatorsky N, Kua L, Naskar D, Teng F, et al. Identifying species of symbiont bacteria from the human gut that, alone, can induce intestinal Th17 cells in mice. Proceedings of the National Academy of Sciences of the United States of America 2016;113(50):E8141-E50.
16. 16. Fan L, Qi Y, Qu S, Chen X, Li A, Hendi M, et al. B. adolescentis ameliorates chronic colitis by regulating Treg/Th2 response and gut microbiota remodeling. Gut Microbes 2021;13(1):1–17.

17. 17. Devi TB, Devadas K, George M, Gandhimathi A, Chouhan D, Retnakumar RJ, et al. Low Bifidobacterium Abundance in the Lower Gut Microbiota Is Associated With Helicobacter pylori-Related Gastric Ulcer and Gastric Cancer. Front Microbiol 2021;12:631140.
18. 18. Sivan A, Corrales L, Hubert N, Williams JB, Aquino-Michaels K, Earley ZM, et al. Commensal Bifidobacterium promotes antitumor immunity and facilitates anti-PD-L1 efficacy. Science 2015;350(6264):1084-9.
19. 19. Thiele Orberg E, Fan H, Tam AJ, Dejea CM, Destefano Shields CE, Wu S, et al. The myeloid immune signature of enterotoxigenic Bacteroides fragilis-induced murine colon tumorigenesis. Mucosal Immunol 2017;10(2):421 – 33.
20. 20. Long X, Wong CC, Tong L, Chu ESH, Ho Szeto C, Go MYY, et al. Peptostreptococcus anaerobius promotes colorectal carcinogenesis and modulates tumour immunity. Nat Microbiol 2019;4(12):2319-30.
21. 21. Shi Y, Zheng W, Yang K, Harris KG, Ni K, Xue L, et al. Intratumoral accumulation of gut microbiota facilitates CD47-based immunotherapy via STING signaling. J Exp Med 2020;217(5).
22. 22. Sahai E, Astsaturov I, Cukierman E, DeNardo DG, Egeblad M, Evans RM, et al. A framework for advancing our understanding of cancer-associated fibroblasts. Nat Rev Cancer 2020;20(3):174 – 86.
23. 23. Yang Y, Weng W, Peng J, Hong L, Yang L, Toiyama Y, et al. Fusobacterium nucleatum Increases Proliferation of Colorectal Cancer Cells and Tumor Development in Mice by Activating Toll-Like Receptor 4 Signaling to Nuclear Factor-kappaB, and Up-regulating Expression of MicroRNA-21. Gastroenterology 2017;152(4):851 – 66 e24.
24. 24. de Vries NL, van Unen V, Ijsselsteijn ME, Abdelaal T, van der Breggen R, Farina Sarasqueta A, et al. High-dimensional cytometric analysis of colorectal cancer reveals novel mediators of antitumour immunity. Gut 2020;69(4):691–703.
25. 25. Lambrechts D, Wauters E, Boeckx B, Aibar S, Nittner D, Burton O, et al. Phenotype molding of stromal cells in the lung tumor microenvironment. Nature medicine 2018;24(8):1277-89.
26. 26. Bian S, Hou Y, Zhou X, Li X, Yong J, Wang Y, et al. Single-cell multiomics sequencing and analyses of human colorectal cancer. Science 2018;362(6418):1060-3.
27. 27. Paulsson J, Micke P. Prognostic relevance of cancer-associated fibroblasts in human cancer. Semin Cancer Biol 2014;25:61 – 8.
28. 28. Ozdemir BC, Pentcheva-Hoang T, Carstens JL, Zheng X, Wu CC, Simpson TR, et al. Depletion of carcinoma-associated fibroblasts and fibrosis induces immunosuppression and accelerates pancreas cancer with reduced survival. Cancer cell 2014;25(6):719 – 34.
29. 29. Mizutani Y, Kobayashi H, Iida T, Asai N, Masamune A, Hara A, et al. Meflin-Positive Cancer-Associated Fibroblasts Inhibit Pancreatic Carcinogenesis. Cancer research 2019;79(20):5367-81.
30. 30. Zhao X, Ding L, Lu Z, Huang X, Jing Y, Yang Y, et al. Diminished CD68(+) Cancer-Associated Fibroblast Subset Induces Regulatory T-Cell (Treg) Infiltration and Predicts Poor Prognosis of Oral Squamous Cell Carcinoma Patients. Am J Pathol 2020;190(4):886 – 99.

31. 31. Ohlund D, Handly-Santana A, Biffi G, Elyada E, Almeida AS, Ponz-Sarvise M, et al. Distinct populations of inflammatory fibroblasts and myofibroblasts in pancreatic cancer. J Exp Med 2017;214(3):579 – 96.
32. 32. Sugimoto H, Mundel TM, Kieran MW, Kalluri R. Identification of fibroblast heterogeneity in the tumor microenvironment. Cancer Biol Ther 2006;5(12):1640-6.
33. 33. Costea DE, Hills A, Osman AH, Thurlow J, Kalna G, Huang X, et al. Identification of two distinct carcinoma-associated fibroblast subtypes with differential tumor-promoting abilities in oral squamous cell carcinoma. Cancer research 2013;73(13):3888 – 901.
34. 34. Bartoschek M, Oskolkov N, Bocci M, Lovrot J, Larsson C, Sommarin M, et al. Spatially and functionally distinct subclasses of breast cancer-associated fibroblasts revealed by single cell RNA sequencing. Nature communications 2018;9(1):5150.
35. 35. Zambidis ET, Park TS, Yu W, Tam A, Levine M, Yuan X, et al. Expression of angiotensin-converting enzyme (CD143) identifies and regulates primitive hemangioblasts derived from human pluripotent stem cells. Blood 2008;112(9):3601-14.
36. 36. Danilov SM, Sadovnikova E, Scharenborg N, Balyasnikova IV, Svinareva DA, Semikina EL, et al. Angiotensin-converting enzyme (CD143) is abundantly expressed by dendritic cells and discriminates human monocyte-derived dendritic cells from acute myeloid leukemia-derived dendritic cells. Exp Hematol 2003;31(12):1301-9.
37. 37. Roberts EW, Deonarine A, Jones JO, Denton AE, Feig C, Lyons SK, et al. Depletion of stromal cells expressing fibroblast activation protein-alpha from skeletal muscle and bone marrow results in cachexia and anemia. J Exp Med 2013;210(6):1137-51.
38. 38. Del Sal G, Ruaro ME, Philipson L, Schneider C. The growth arrest-specific gene, gas1, is involved in growth suppression. Cell 1992;70(4):595–607.
39. 39. Li Q, Qin Y, Wei P, Lian P, Li Y, Xu Y, et al. Gas1 Inhibits Metastatic and Metabolic Phenotypes in Colorectal Carcinoma. Mol Cancer Res 2016;14(9):830 – 40.
40. 40. Grauel AL, Nguyen B, Ruddy D, Laszewski T, Schwartz S, Chang J, et al. TGFbeta-blockade uncovers stromal plasticity in tumors by revealing the existence of a subset of interferon-licensed fibroblasts. Nature communications 2020;11(1):6315.
41. 41. Nielsen SR, Quaranta V, Linford A, Emeagi P, Rainer C, Santos A, et al. Macrophage-secreted granulin supports pancreatic cancer metastasis by inducing liver fibrosis. Nat Cell Biol 2016;18(5):549 – 60.
42. 42. Lee CS, Buttitta L, Fan CM. Evidence that the WNT-inducible growth arrest-specific gene 1 encodes an antagonist of sonic hedgehog signaling in the somite. Proceedings of the National Academy of Sciences of the United States of America 2001;98(20):11347-52.
43. 43. Bugter JM, Fenderico N, Maurice MM. Mutations and mechanisms of WNT pathway tumour suppressors in cancer. Nat Rev Cancer 2021;21(1):5–21.
44. 44. Mosa MH, Michels BE, Menche C, Nicolas AM, Darvishi T, Greten FR, et al. A Wnt-Induced Phenotypic Switch in Cancer-Associated Fibroblasts Inhibits EMT in Colorectal Cancer. Cancer

research 2020;80(24):5569-82.

Figures

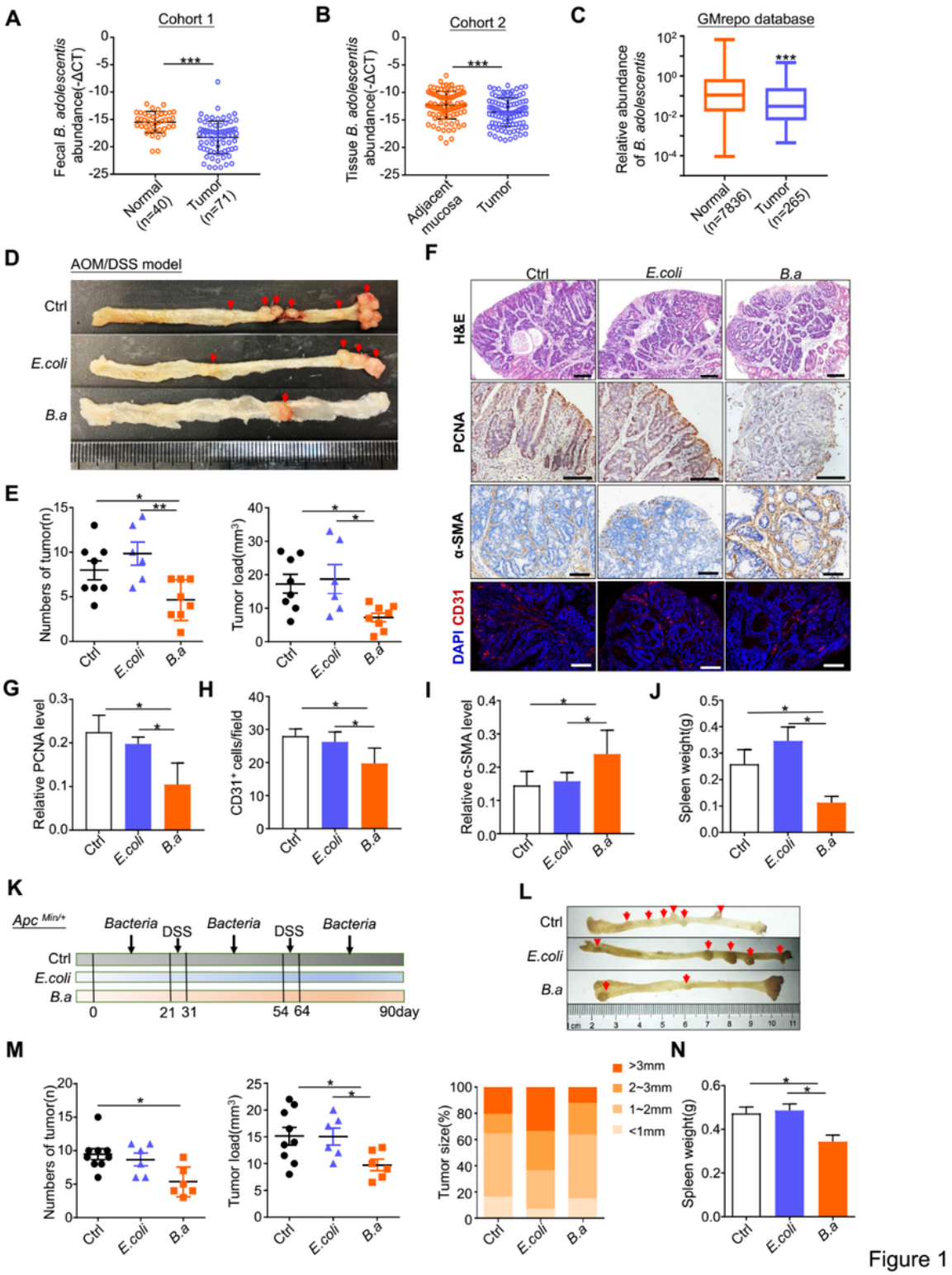

Figure 1

Figure 1

B. adolescentis was decreased in CRC patients and suppressed tumorigenesis in mice. **a** Fecal bacterial genomic DNA was extracted from healthy individuals (Normal, n=40) and patients with CRC (Cancer, n=71) in cohort 1. The expression of *B. adolescentis* was determined by *qRT-PCR*. **b** Bacterial genomic DNA was extracted from CRC tissues and adjacent normal mucosa (n=99) (cohort 2). The expression of *B. adolescentis* was tested by *qRT-PCR.* **c** The relative fecal abundance of *B. adolescentis* in healthy individuals (Normal, n=7836) and patients with CRC (Cancer, n=265) in the GMrepo database. **d** Representative colon images of AOM/DSS mice treated with *B. adolescentis* (*B.a*) (n=8), *E.coli* (n=6) or PBS (n=8) as control. The red arrows indicate the tumor locations. **e** Tumor number and tumor load in the colorectum were measured. **f** Representative images of H&E staining, immunostaining for PCNA or α-SMA and immunofluorescence staining for CD31 in CRC tissues. White scale bars, 500 μm, black scale bars, 100 μm. The qualitative expression of (**g**)PCNA, (**h**) α-SMA and (**i**) CD31 were analyzed. **j** Spleen weights were measured. **k** Experimental model in $Apc^{Min/+}$ mice. **l** Representative colon images of $Apc^{Min/+}$ mice treated with *B. adolescentis* (*B.a*) (n=6), *E.coli* (n=6) or PBS (n=9) as control. **m** Tumor number, size, and load in the colorectum were measured. **n** Spleen weights were measured. Data are presented as mean ± SD. *, P <0.05, **, P <0.01, ***, P <0.001, Kruskal-Wallis test (a), Mann-Whitney test (b), Wilcoxon matched-pairs signed-rank test (c) and ANOVA test (e-j).

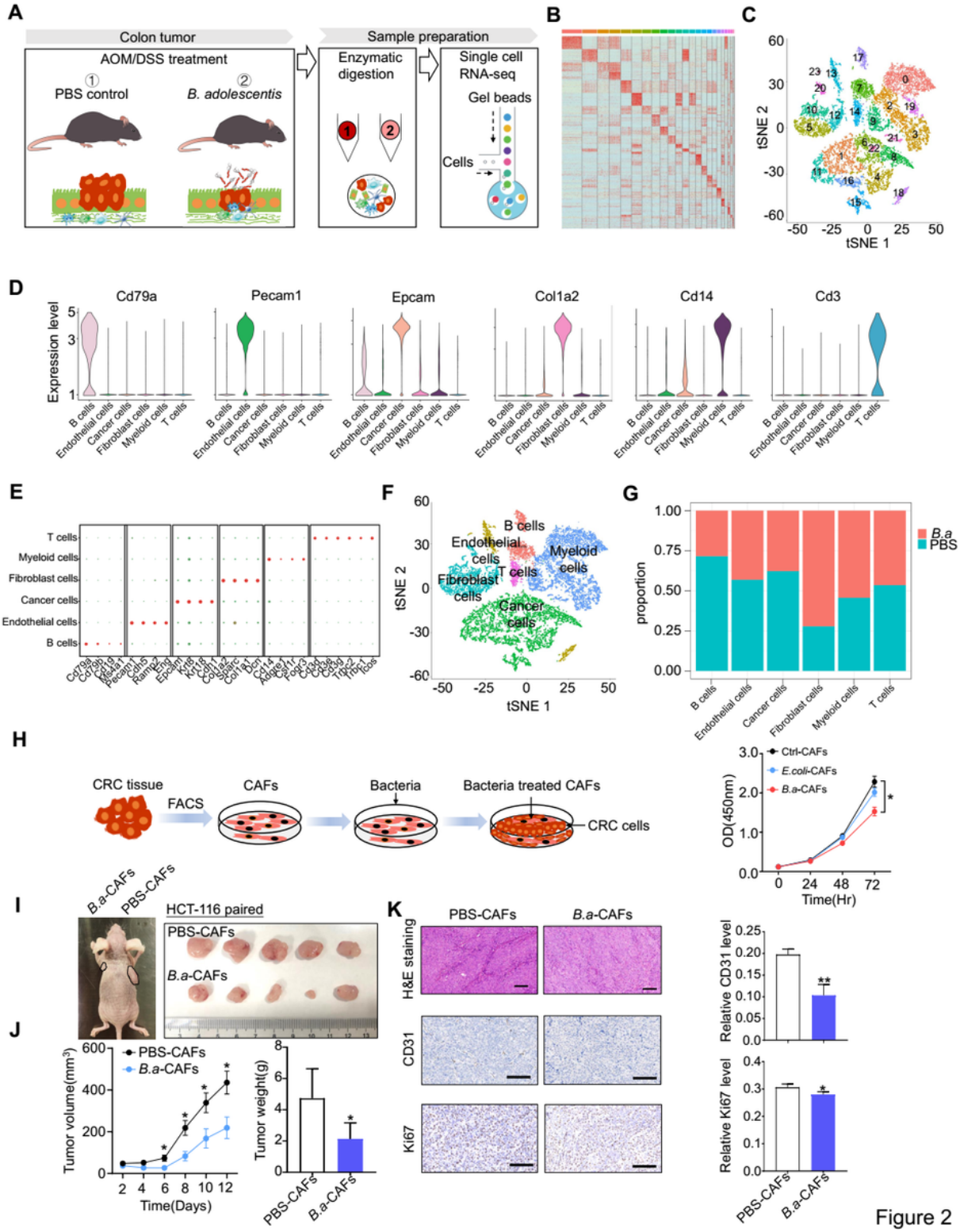

Figure 2

Figure 2

B. adolescentis recruited fibroblasts to suppress colonic tumorigenesis. **a** The pattern diagram for the single cell preparation and single cell RNA-sequencing. **b,c** Unsupervised graph clustering divided infiltrating cells into 24 groups based on gene expression pattern and groups were plotted in t-SNE. **d-f** Cells were divided into 6 groups according to their top expression markers. **g** The percentage of 6 groups in PBS and *B.a* groups respectively. **h** Primary CAFs were isolated from the CRC tumor and incubated with

B. adolescentis for 48 h, followed by co-cultured with HCT-116 cells, then the cell viability was evaluated at 24, 48 and 72 h by CCK-8 assay. HCT-116 cells were mixed with *B.a* treated-CAFs (MOI=10:1) or PBS treated-CAFs and then injected subcutaneously into the nude mice. The representative tumor images were shown (**i**) and the tumor volume and weight were recorded (**j**). **k** The expression levels of Ki67 and CD31 in the tumor from PBS control (Ctrl) or *B.a* nude mice were examined by immunostaining, Scale bars, 100 μm. The independent experiment was repeated for three times. Data are presented as mean ±SD, n=6. *, *P* <0.05, **, *P* <0.01, ANOVA test (h) or student t test (j,k).

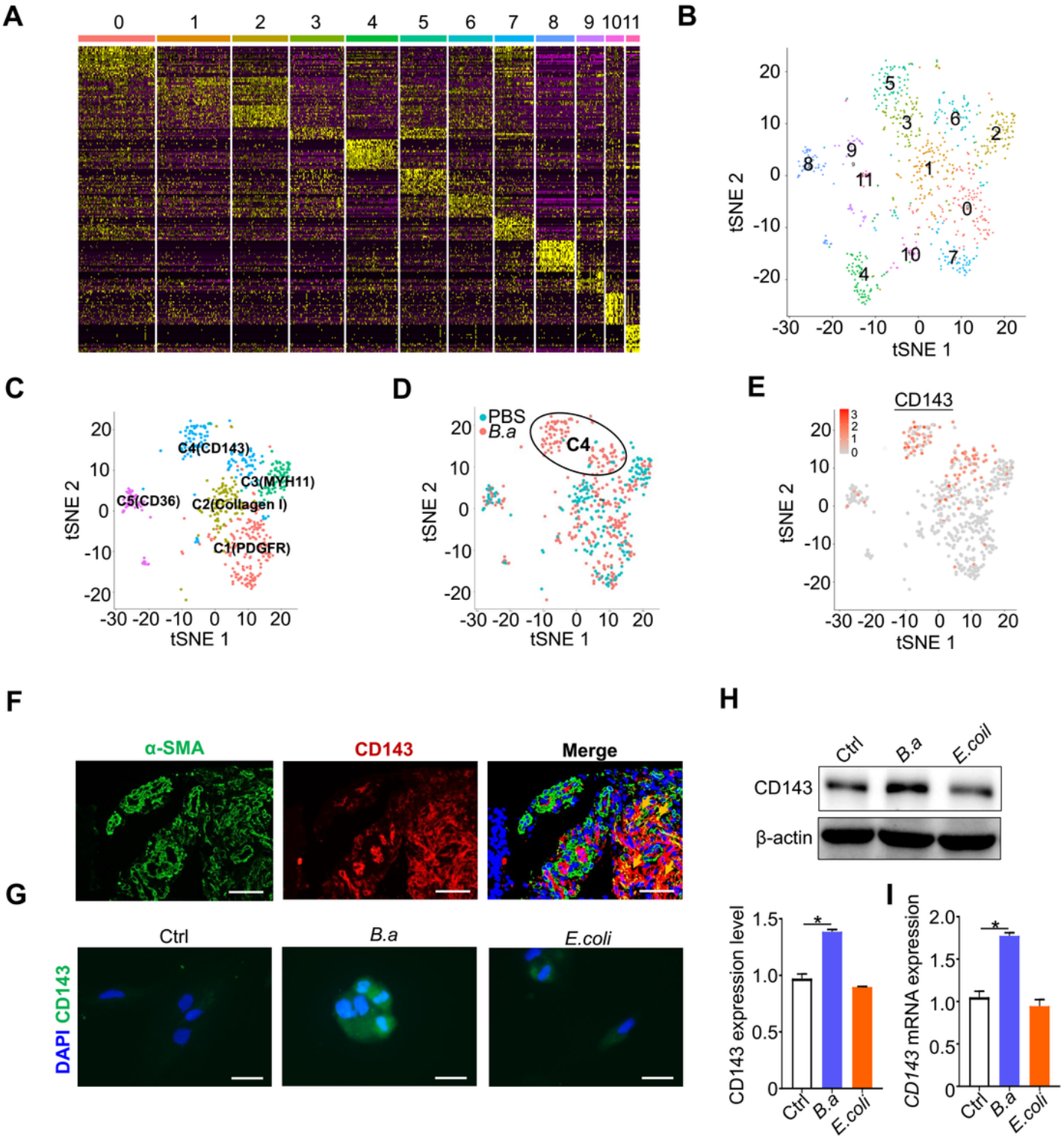

Figure 3

$CD143^+$ CAFs was activated by *B. adolescentis in vivo* and *in vitro.* (**a,b**) Unsupervised graph clustering divided the fibroblasts group into 12 groups based on gene expression pattern and groups were plotted in t-SNE. **c** 5 CAFs groups of C1(PDGFRβ), C2(collagen I), C3(MYH11), C4(CD143), C5(CD36) were analyzed according to the surface markers. **d** t-SNE showed the location of all CAFs cells in the *B.a* and PBS groups. **e** t-SNE showed the CAFs cells with the high expression of CD143. **f** The immunofluorescence staining for the dual α-SMA and CD143 positive cells in the tumor tissue from CRC patients. Scale bars, 100 μm. The yellow arrows indicate the positively stained cells. Primary CAFs were isolated from the CRC tumor and incubated with *B. adolescentis* or *E.coli* for 48 h, then the protein expression of CD143 were shown by immunofluorescence staining (**g**) and western blot (**h**), the mRNA expression was shown by qPCR (**i**). Scale bars, 50 μm. The independent experiment was repeated for three times. Data are presented as mean ±SD. *, P <0.05, ANOVA test (h,i).

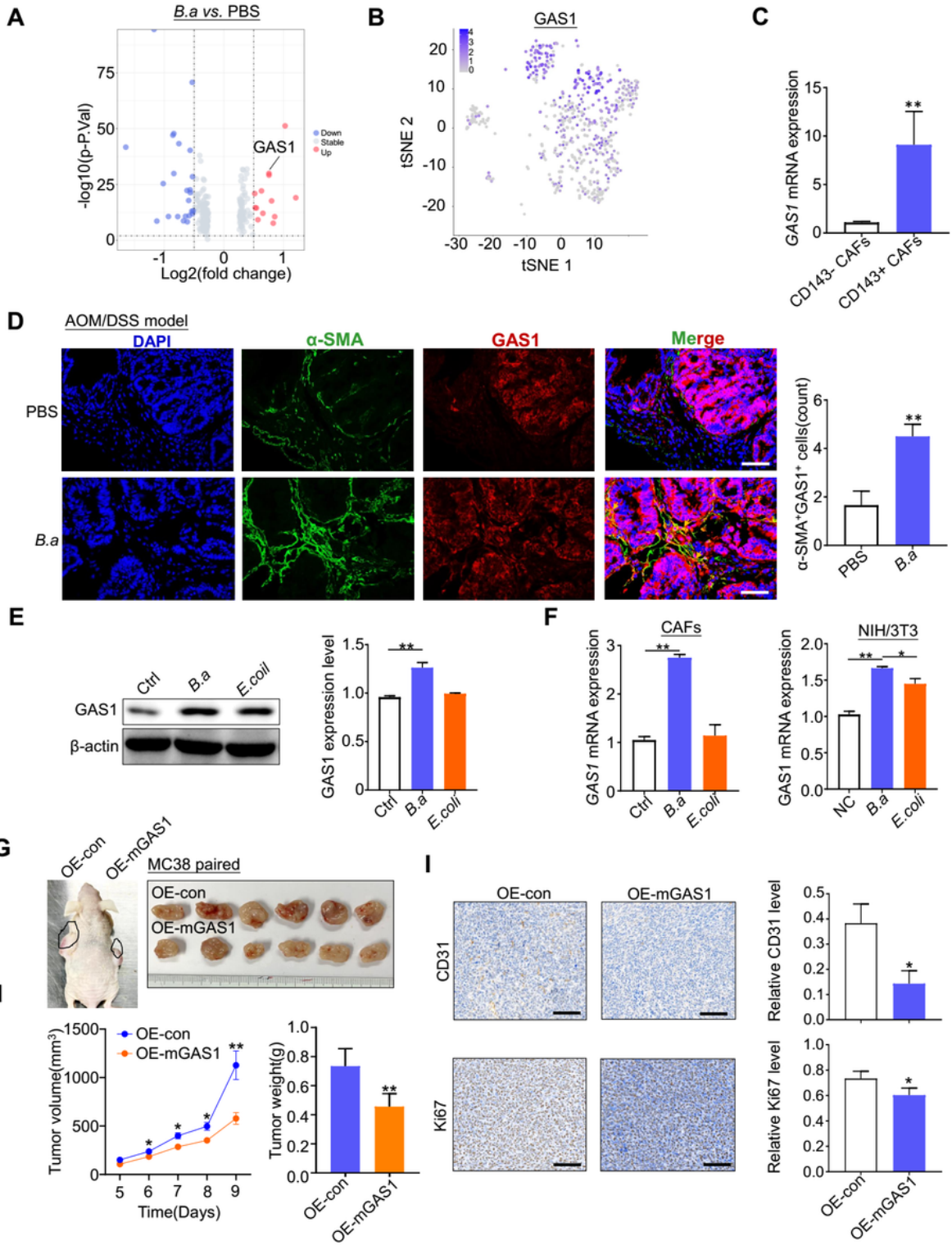

Figure 4

CD143^{+} CAFs was highly expressed with GAS1 in response to *B. adolescentis* treatment. **a** Different gene expression (DGE) between the colon tumors from the PBS and *B.a* groups with AOM/DSS treatment. **b** t-SNE showed the CAFs cells with the high expression of GAS1. **c** RNA sequencing showed the relative expression of GAS1 in CD143^{-} CAFs and CD143^{+} CAFs. **d** The immunofluorescence staining for the dual α-SMA and GAS1 positive cells in the tumor tissue from AOM/DSS mice. Scale bars, 100 μm. The yellow

arrows indicate the positively stained cells. Primary CAFs were isolated from the CRC tumor and incubated with *B. adolescentis* or *E.coli* for 48 h, then the protein expression of GAS1 were shown by western blot (**e**), and the mRNA expression of GAS1was shown by qPCR (**f**). **g-h** MC38 cells were mixed with GAS1-overexpressed NIH/3T3 (MOI=10:1) or OE-con NIH/3T3 and then injected subcutaneously into the nude mice. The representative tumor images were shown (**g**) and the tumor volume and weight were recorded (**h**). **i** The expression levels of Ki67 and CD31 in the tumor from control (OE-con) or OE-mGAS1 nude mice were examined by immunostaining, Scale bars, 100 μm. The independent experiment was repeated for three times. Data are presented as mean ±SD. **, *P* <0.01, student t test (c,d), ANOVA test (e,f).

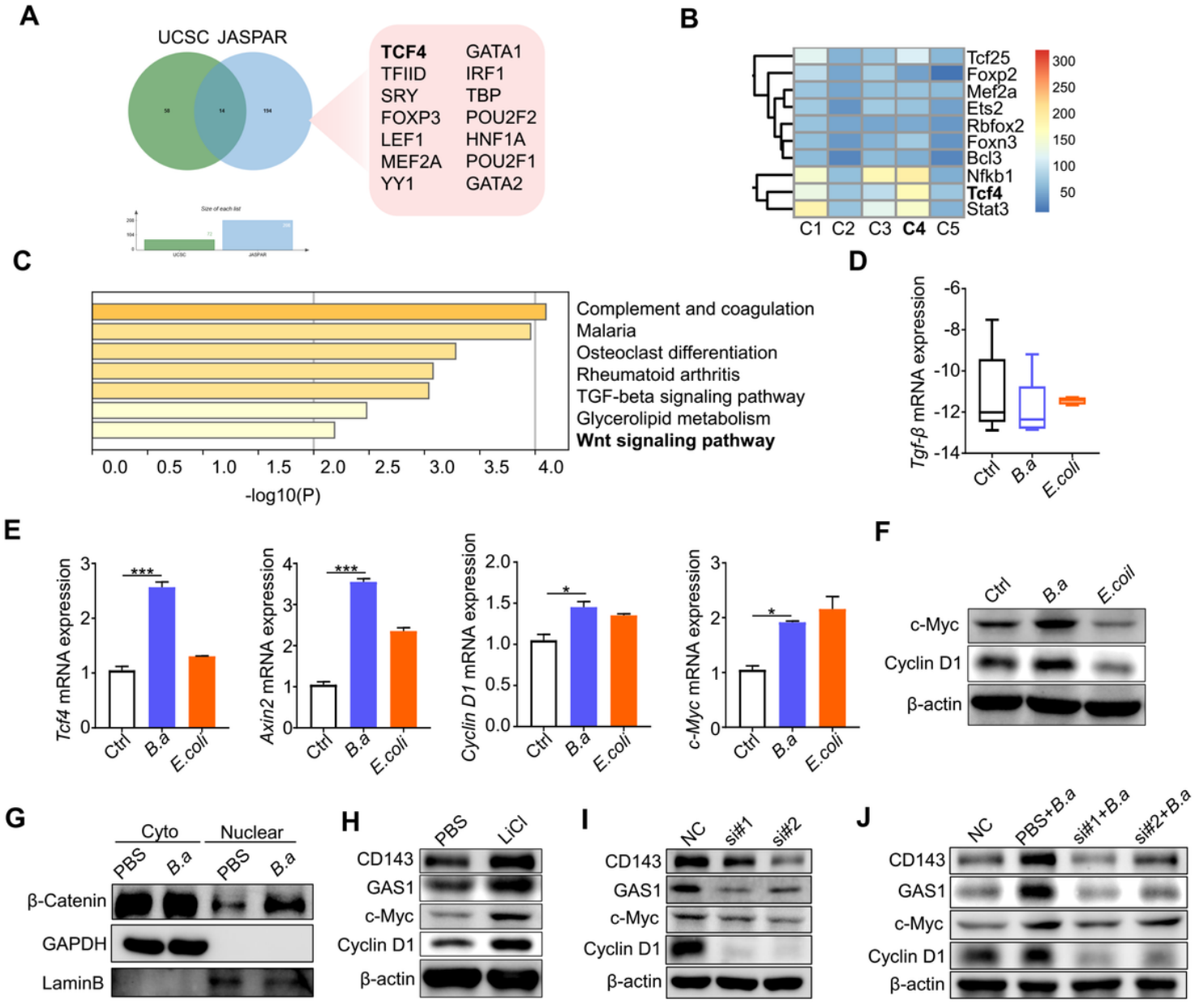

Figure 5

Wnt/β-catenin signaling involved in the induction of CD143$^+$ CAFs by *B. adolescentis*. **a** The online translatory predictor datasets of UCSC and JASPAR predicted the merged translatory genes of GAS1. **b** The DGE of the translator factors between the 5 CAF subsets. **c** The KEGG pathway was enriched in the subset of C4 (CD143$^+$ CAFs). **d** The mRNA expression level of *Tgf-β* in the tumor tissues from the AOM/DSS mice was confirmed by *qPCR*. **e** The CAFs were co-cultured with *B. adolescentis* or *E. coli* for 48 h, then the relative expression of *Tcf4*, *Axin2*, *Cyclin D1* and *c-Myc* were examined by *qPCR*. **f** The relative protein expression of c-Myc and Cyclin D1 were tested by western blot. **g** Nuclear and cytoplasmic separation assay was performed to isolate the nuclear and cytoplasm, then western blot showed the protein expression of β-catenin in the nuclear and cytoplasm. **h** CAFs were incubated with Wnt signaling agonist lithium chloride (LiCl) (20 mmol/L) for 48 h, then the expression of c-Myc, Cyclin D1 and GAS1 were analyzed by western blot. **i** TCF4 deficiency in CAFs was performed by siRNA assay, then the expression of c-myc, Cyclin D1 and GAS1 were examined by western blot. **j** TCF4 deficient CAFs or wildtype CAFs were co-cultured with *B. adolescentis* for 48 h, then the Wnt/β-catenin pathway of c-Myc, Cyclin D1 and GAS1 were tested by western blot. The independent experiment was repeated for three times. Data are presented as mean ±SD. *, P <0.05, **, P <0.01, ***, P <0.001, ANOVA test (e).

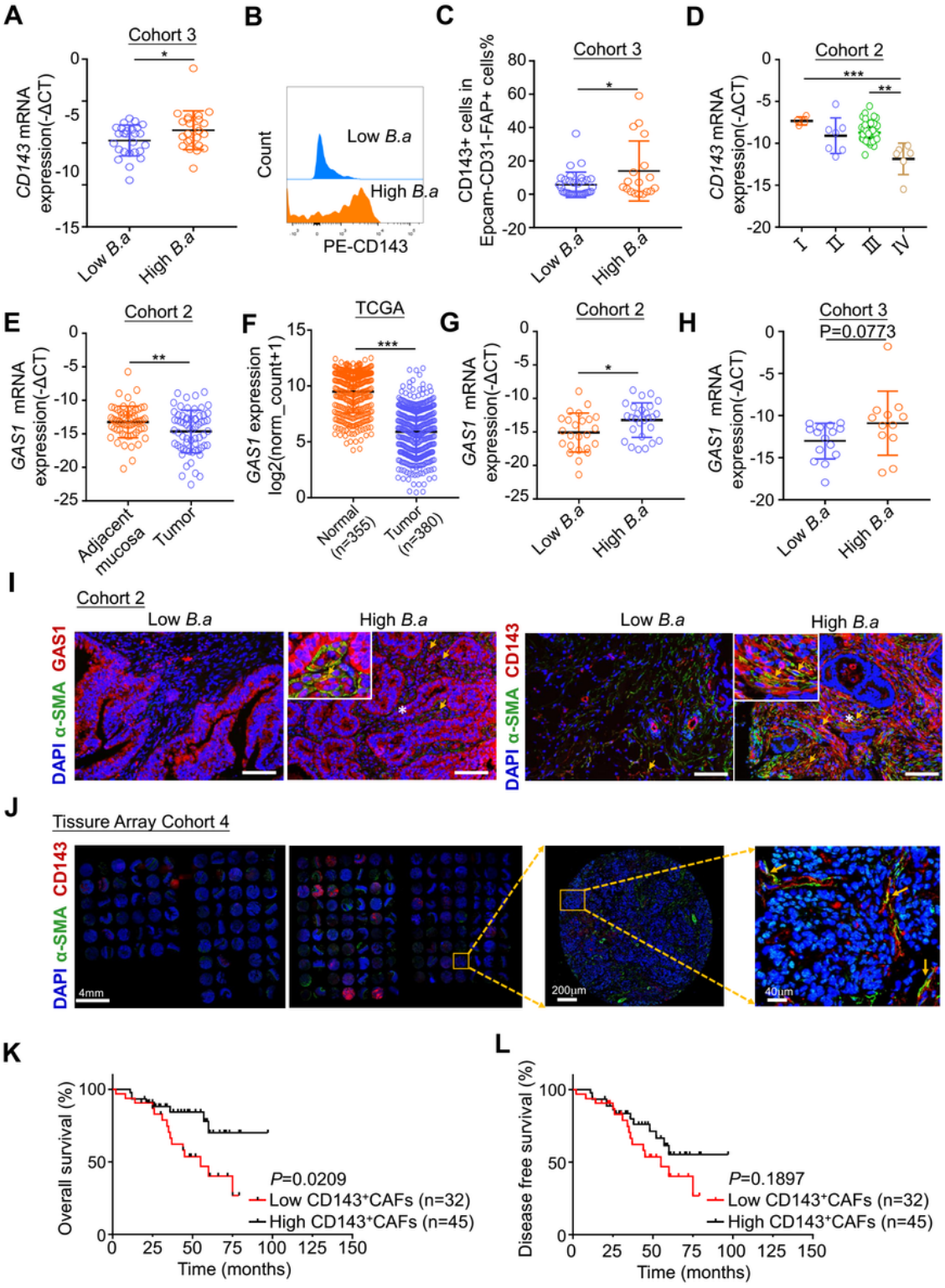

Figure 6

CD143^{+}CAFs predicated better survival in CRC patients *and B. adolescentis* abundance was correlated with the expression of CD143 and GAS1. **a** Cohort 3 was divided into two groups with low and high abundance of *B. adolescentis* by the DNA level (-ΔCT =-15), then the mRNA expression level of CD143 in low and high *B. a* groups was tested by *qPCR*. **b,c** The percentage of CD143^{+}CAFs(CD143^{+}FAP^{+}Epcam^{-} CD31^{-} cell) in the low or high *B. a* abundance was analyzed by flow cytometry. **d** The expression level of

CD143 in the different stage of CRC in the cohort 2 was tested by *qPCR*. **e** The relative expression of GAS1 in cancer tissue and its normal tissue from the cohort 2 were explored by *qPCR*. **f** Expression of GAS1 in colorectal cancer tissue and normal tissue in TCGA TARGET GTEx datasets. **g,h** The relative abundance of GAS1 in low or high *B. a* groups from the cohort 2 and cohort 3 were tested by *qPCR*. **i** The immunofluorescence staining for the dual α-SMA and GAS1 positive cells or α-SMA and CD143 positive cells in the tumor tissue from cohort 2. Scale bars, 100 μm. **j** CRC tissue sections of 80 samples from the tissue array cohort 4 were stained with antibodies for α-SMA and CD143. yellow arrows indicate target cells. Scale bars were shown in the pictures. **k,l** The Kaplan–Meier survival curves/log-rank tests were used to compare overall survival (**k**) and disease free survival (**l**) in groups with high and low numbers of CD143+CAFs. Data are presented as mean ±SD. *, P <0.05, ***, P <0.001, Kruskal-Wallis test (d), Mann-Whitney test (a,c,f,g,h), Wilcoxon matched-pairs signed-rank test (e), log-rank tests(k,l).

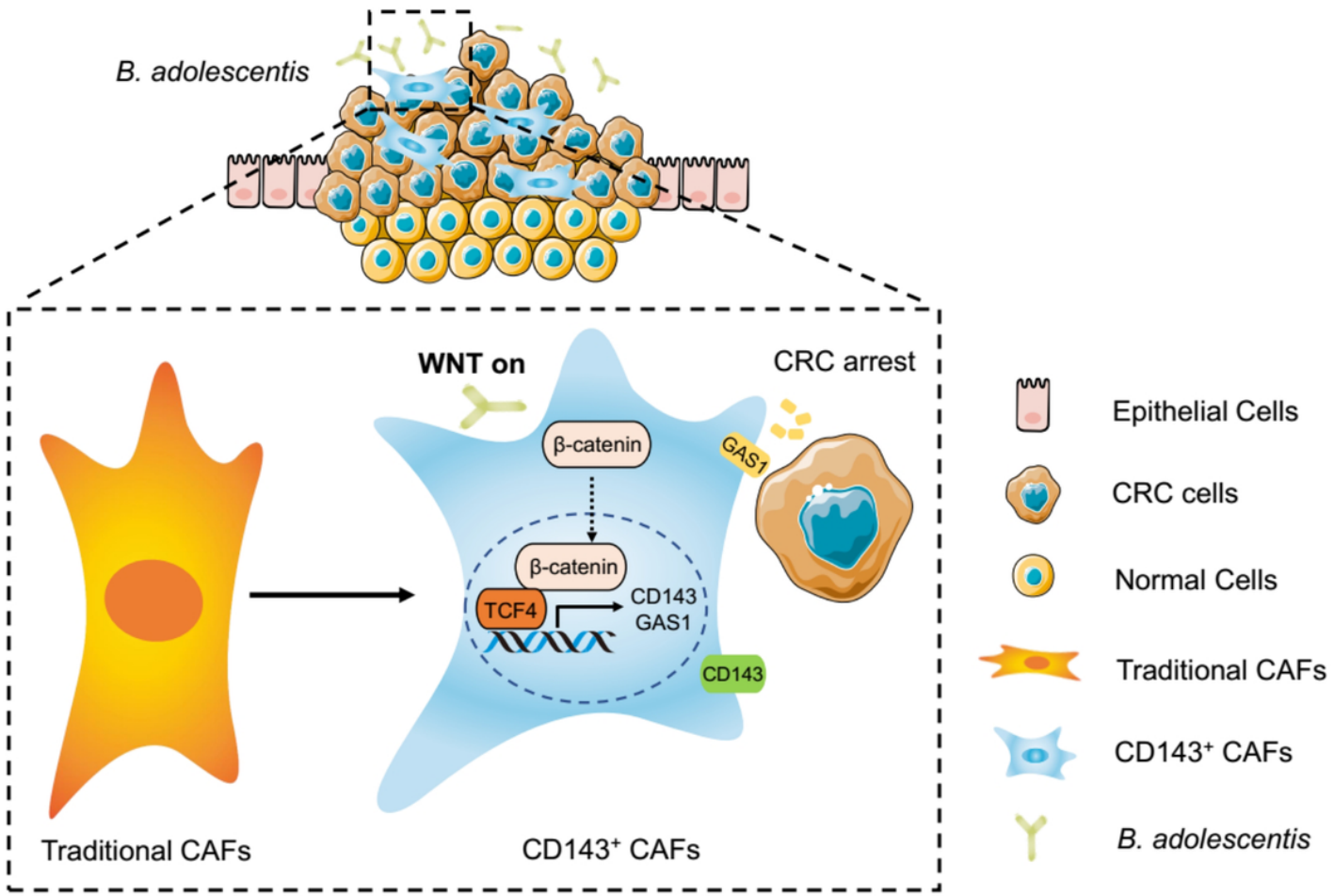

Figure 7

The pattern model of *B. adolescentis* regulating CRC progression.